Chinese Chemical Letters 36 (2025) 110295

Contents lists available at ScienceDirect

Chinese Chemical Letters

journal homepage: www.elsevier.com/locate/cclet

Improved N_2 selectivity for low-temperature NO_x reduction over etched ZSM-5 supported MnCe oxide catalysts

Shanyuan Bi[1], Jin Zhang[1], Dengchao Peng, Danhong Cheng, Jianping Zhang*, Lupeng Han*, Dengsong Zhang*

International Joint Laboratory of Catalytic Chemistry, State Key Laboratory of Advanced Special Steel, Innovation Institute of Carbon Neutrality, Department of Chemistry, College of Sciences, Shanghai University, Shanghai 200444, China

ARTICLE INFO

Article history:
Received 16 March 2024
Revised 25 June 2024
Accepted 24 July 2024
Available online 25 July 2024

Keywords:
NO_x
Selective catalytic reduction
Mn-based catalyst
Low-temperature activity
N_2 selectivity

ABSTRACT

Developing a high-efficiency catalyst with both superior low-temperature activity and good N_2 selectivity is still challenging for the NH_3 selective catalytic reduction (SCR) of NO_x from mobile sources. Herein, we demonstrate the improved low-temperature activity and N_2 selectivity by regulating the redox and acidic properties of MnCe oxides supported on etched ZSM-5 supports. The etched ZSM-5 enables the highly dispersed state of $MnCeO_x$ species and strong interaction between Mn and Ce species, which promotes the reduction of CeO_2, facilitates electron transfer from Mn to Ce, and generates more Mn^{4+} and Ce^{3+} species. The strong redox capacity contributes to forming the reactive nitrate species and -NH_2 species from oxidative dehydrogenation of NH_3. Moreover, the adsorbed NH_3 and -NH_2 species are the reactive intermediates that promote the formation of N_2. This work demonstrates an effective strategy to enhance the low-temperature activity and N_2 selectivity of SCR catalysts, contributing to the NO_x control for the low-temperature exhaust gas during the cold-start of diesel vehicles.

Nitrogen oxides (NO_x) emitted from diesel engines account for a considerable portion of air pollutant emissions, which leads to a string of ecological environmental issues in the case of the formation of acid rain, photochemical smog, and haze [1-3]. Currently, selective catalytic reduction with NH_3 (NH_3-SCR) is a widely applied technology to eliminate nitrogen oxide originating from diesel vehicle exhaust [4-6]. As the core of this technology, catalysts have attracted much attention from researchers [4,7,8]. Metal oxide, noble metal, transition metal, and zeolite catalysts are widely researched by scientists [9-11]. Among them, Cu-SSZ-13 is a commercially available catalyst widely used in removing NO_x from diesel vehicles owing to its superior SCR activity and hydrothermal stability [12,13]. Nevertheless, there remains a critical challenge to achieving the goal of rigorous emission control in the future. Considering its higher light-off (>150 °C) temperature, the Cu-SSZ-13 catalyst is unable to effectively remove NO_x during the low temperature below 200 °C [14]. Hence, it is necessary to explore a high-efficiency SCR catalyst for the low-temperature exhaust gas during the cold-start of diesel vehicles [14,15].

Compared with commercial Cu-SSZ-13 catalysts, ZSM-5-based catalysts have more environmentally friendly and low-cost synthesis approaches, which exhibit broad application prospects [16,17]. Developing highly efficient ZSM-5-based catalysts has attracted much attention [18-20]. Fe, Cu-based ZSM-5 catalysts are the most extensively researched [21-24]. However, the low-temperature activity of Fe-ZSM-5 and Cu-ZSM-5 is generally not satisfactory with T_{90} around 300 °C and 250 °C, respectively [25,26]. Manganese oxide-based catalysts have been demonstrated to possess excellent low-temperature activity owing to the variable valence states (Mn^{4+}, Mn^{3+}, and Mn^{2+}) and excellent redox capacity [27]. Therefore, manganese oxide modification is a good strategy to improve the ZSM-5 catalysts' low-temperature activity. Ji *et al.* developed a novel CeMn-ZSM-5 heterogeneous catalyst by simple mechanical grinding of CeMn oxides and ZSM5, which showed beyond 90% NO_x conversion during 100–250 °C [28]. However, N_2 selectivity of CeMn-ZSM-5 was below 90% above 180 °C. Chen *et al.* constructed Mn-Ce/ZSM-5 catalyst by an impregnation method, which showed above 90% NO_x conversion from 210 °C to 300 °C but low N_2 selectivity below 90% above 200 °C [29]. Zhou *et al.* found that Fe-Ce-Mn/ZSM-5 delivers over 95% NO_x conversion between 200 °C and 360 °C. Whereas, with the increasing temperature, a large amount of N_2O was produced along with the gradual decrease of N_2 selectivity [30]. From the above results, the strong oxidizing

* Corresponding authors.
E-mail addresses: wjpzjp@shu.edu.cn (J. Zhang), lphan@shu.edu.cn (L. Han), dszhang@shu.edu.cn (D. Zhang).
[1] These authors contributed equally to this work.

https://doi.org/10.1016/j.cclet.2024.110295
1001-8417/

property of Mn-based catalysts undoubtedly leads to worse N_2 selectivity at high temperatures resulting from the excessive oxidation of NH_3 [31]. Therefore, it is urgent to enhance N_2 selectivity of Mn-based ZSM-5 catalysts and simultaneously maintain good low-temperature activity.

Creating more mesopores in ZSM-5 is a valid method to enhance catalyst activity by providing more access to available catalytically active sites [24,32,33]. The high specific surface area and porosity of mesoporous ZSM-5 help the active sites to be more dispersed and facilitate the complexation with metal oxides [34,35]. The alkali treatment of microporous ZSM-5 is a simple and effective method to remove the silicon of ZSM-5 framework and introduce mesoporous [37]. In this work, we treated the ZSM-5 zeolite with an etching method using a mixed-alkaline solution (NaOH and TMAH) to create more mesopores, named Z5-E. Then Mn and Ce metal oxides were introduced into Z5-E by an impregnation method to obtain the MnCe/Z5-E catalyst. Interestingly, MnCe/Z5-E possesses more than 90% NO_x conversion from 180 °C to 330 °C, which exhibits superior low-temperature activity than the Cu-SSZ-13 commercial catalyst. Moreover, MnCe/Z5-E shows good N_2 selectivity with more than 90% below 270 °C and more than 80% below 360 °C. As a comparison, the unetched MnCe/Z5 catalyst shows similar low-temperature activity but inferior N_2 selectivity. The promotion mechanism of the low-temperature activity and N_2 selectivity over MnCe/Z5-E is probed by the detailed characterizations in terms of the acidic and redox properties of catalysts.

The Z5-E zeolite introduced more mesopores *via* mixed-alkaline etching: Add a certain quantity of Z5 zeolite after dissolving a certain quantity of NaOH and TMAH (provided by Sinopharm Chemical Reagent Co., Ltd. (China)) in deionized water, after etching for 0.5 h in 90 °C oil-bath, centrifuge and wash with deionized water until neutral, and then dry in 80 °C oven overnight, calcine the dried samples to acquire Z5-E zeolite. MnCe/Z5-E and MnCe/Z5 were prepared by impregnation method: Add a quantity of $Mn(CH_3COO)_2{\cdot}4H_2O$ and $Ce(NO_3)_3{\cdot}6H_2O$ (provided by Sinopharm Chemical Reagent Co., Ltd. (China)) after dissolving in anhydrous ethanol to Z5-E and Z5, respectively, remove the superfluous solution by 45 °C rotary evaporation, then dry in 80 °C oven and calcine at 500 °C for 6 h to acquire MnCe/Z5-E and MnCe/Z5. More detailed experimental parameters and characterizations were provided in the Supporting information.

Firstly, the NH_3-SCR activity and N_2 selectivity of unetched Mn/Z5 and Ce/Z5 were compared with unetched MnCe/Z5 (Fig. S1 in Supporting information). The low-temperature activity of Mn/Z5 is not as good as that of MnCe/Z5 and produces a large amount of N_2O (up to 290 ppm). Compared with MnCe/Z5, Ce/Z5 has worse low-temperature activity but better N_2 selectivity. Although the unetched MnCe/Z5 shows good low-temperature activity with 85% NO_x conversion at 180 °C, N_2 selectivity is below 90% above 180 °C with a large amount of N_2O production (up to 105 ppm) above 240 °C. In order to improve N_2 selectivity, we prepared etched MnCe/Z5-E and investigated the effects of MnCe loadings, solvent, and etching time of ZSM-5 on the activity and N_2 selectivity (Figs. S2, S4, S6, and S7 in Supporting information). From both points of NO_x conversion and N_2 selectivity, MnCe/Z5-E using anhydrous ethanol as a solvent with 15 wt% MnO_2 and 10 wt% CeO_2 and the etching time of 0.5 h is the optimum catalyst (shortly denoted as MnCe/Z5-E in the following context). Besides, MnCe/Z5 with 15 wt% MnO_2 and 10 wt% CeO_2 is also the optimum catalyst (Figs. S3 and S5 in Supporting information). Compared with the unetched MnCe/Z5, the etched MnCe/Z5-E catalyst not only shows higher low-temperature activity but much better N_2 selectivity, as seen in Fig. 1. MnCe/Z5-E exhibits above 90% NO_x conversion with a broad window of 180–330 °C, which shows much better low-temperature activity than the commercial Cu-SSZ-13 (Fig. 1a). Interestingly, the production of N_2O of MnCe/Z5-E is notably inhibited compared

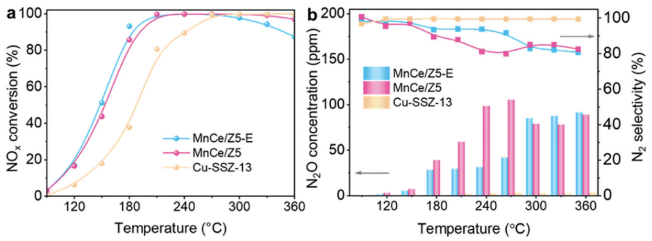

Fig. 1. (a) NO_x conversion, (b) N_2O concentration (histogram) and N_2 selectivity (line chart) as a function of reaction temperature for the MnCe/Z5-E, MnCe/Z5, and Cu-SSZ-13 catalysts. Reaction conditions: $[NO]=[NH_3]=500$ ppm, $[O_2]=10$ vol%, $[H_2O]=5$ vol%, $[CO_2]=5$ vol%, N_2 as balance gas, and WHSV = 200,000 mL g^{-1} h^{-1}.

with MnCe/Z5, and the generation of N_2O is always below 100 ppm within the whole temperature window (Fig. 1b). N_2 selectivity of MnCe/Z5-E is more than 90% below 270 °C and above 80% within the whole temperature window (Fig. 1b). These results indicate that the production of N_2O is reduced and N_2 selectivity is improved after the mixed-alkaline etching. To investigate the products of non-selective oxidation of NH_3, the experiment of NH_3 oxidation was carried out (Figs. S9 and S10 in Supporting information). The NH_3 conversion of the MnCe/Z5-E is similar to that of the MnCe/Z5. However, the MnCe/Z5 produces a large amount of N_2O, NO, and NO_2 compared to the MnCe/Z5-E, which leads to the poor N_2 selectivity of the MnCe/Z5. Furthermore, even after severe hydrothermal aging treatment, MnCe/Z5-E still shows more than 80% conversion within 210–360 °C while N_2 selectivity keeps above 80% with below 30 ppm N_2O formation for the whole temperature window (Fig. S11 in Supporting information), indicating that the catalyst has excellent hydrothermal stability.

To probe the role of mixed-alkaline etching in improving N_2 selectivity, a series of characterizations and analyses were carried out subsequently. Firstly, the catalyst structure was investigated on MnCe/Z5 and MnCe/Z5-E by XRD experiments. As seen in Fig. 2a, MnCe/Z5 exhibits the XRD peaks of ZSM-5 zeolites mainly at 7.9°, 8.8°, 20.3°, 23.2° and 24.0° (PDF #44-0003) [36]. The ZSM-5 characteristic peaks are all well retained but the intensity is decreased over MnCe/Z5-E. The crystallinity of ZSM-5 decreases because the silica is partially removed in the zeolite framework as

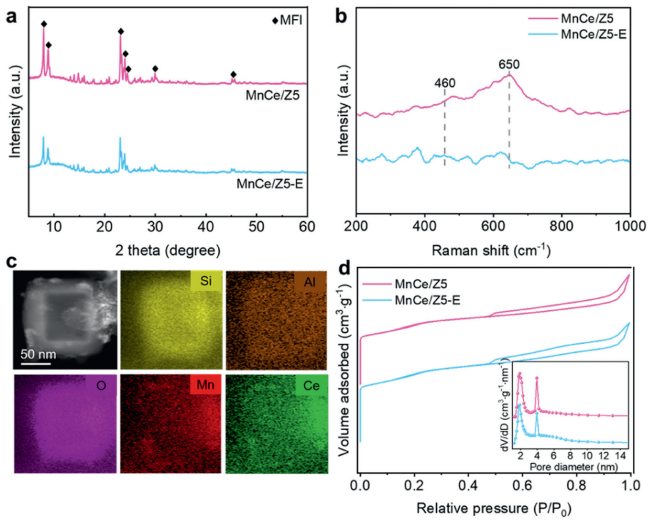

Fig. 2. (a) XRD patterns of MnCe/Z5-E and MnCe/Z5 catalysts. (b) Raman spectra of MnCe/Z5-E and MnCe/Z5 catalysts. (c) STEM images and the corresponding EDX element mapping of Mn, Ce, Si, Al, and O elements for MnCe/Z5-E catalyst. (d) N_2 adsorption-desorption isotherms and pore size distribution (insert) of MnCe/Z5-E and MnCe/Z5 catalysts.

evidenced in the ICP results (Table S1 in Supporting information) [37]. Besides, no characteristic diffraction peaks of $MnCeO_x$ species were found over both MnCe/Z5-E and MnCe/Z5, which indicates the high dispersion of $MnCeO_x$ species or amorphous. Raman spectroscopy was used to investigate further details about the catalyst structure. As seen in Fig. 2b, both catalysts show two bands, in which the peaks at 460 cm^{-1} are assigned to the F_{2g} vibration pattern of CeO_2 fluorite structure, and the peaks at 650 cm^{-1} belong to the Mn-O vibrating in the [MnO_6] octahedra [38,39]. It can be found that MnCe/Z5-E shows weaker intensity of two peaks than MnCe/Z5, indicating the more dispersed state of $MnCeO_x$ species [40]. The morphology of catalysts was investigated using HRTEM. MnCe/Z5 possesses a smooth surface while MnCe/Z5-E shows porous structures (Fig. S12 in Supporting information). EDX was tested to investigate the element dispersion on the surface of catalysts. The distribution of Mn, Ce, Si, Al, and O elements in MnCe/Z5-E are homogeneous, indicating that MnCe oxides are highly dispersed on the catalyst surface (Fig. 2c). However, MnCe oxides are distributed unevenly and clustered together on the surface of MnCe/Z5 (Fig. S13 in Supporting information). The etched MnCe/Z5 has a higher surface area and more mesopores (Fig. 2d and Table S2 in Supporting information) and thus MnCe oxides are not seriously agglomerated.

The redox characteristics of the catalysts play an essential role in SCR reaction. H_2-TPR tests were performed to evaluate the redox properties of the catalysts. As can be seen from Fig. 3a, MnCe/Z5-E and MnCe/Z5 show four reduction peaks that can be divided into the reduction of four oxide species as follows: $MnO_2 \rightarrow Mn_2O_3$, $Mn_2O_3 \rightarrow Mn_3O_4$, $Mn_3O_4 \rightarrow MnO/CeO_2 \rightarrow CeO_x$, and $CeO_2 \rightarrow CeO_x$ along with the elevating reduction temperature [29,31,41]. The total consumption of H_2 is similar for MnCe/Z5-E (0.53 mmol/g) and MnCe/Z5 (0.63 mmol/g), while the proportion of reducible MnO_x species is largely different (Table S3 in Supporting information). The proportion of reducible MnO_2 over MnCe/Z5-E (37.7%) is higher than that over MnCe/Z5 (12.7%). Meanwhile, the proportion of reducible Mn_2O_3 over MnCe/Z5-E (51.0%) is lower than that over MnCe/Z5 (76.2%). These results indicate that more high-valence of Mn species exist on MnCe/Z5-E. It is notable that the proportion of $Mn_3O_4 \rightarrow MnO/CeO_2 \rightarrow CeO_x$ over MnCe/Z5-E (11.2%) is higher than that (4.8%) over MnCe/Z5, which likely account for the more reduction of CeO_2. This also indicates the stronger interaction between Mn and Ce species over MnCe/Z5-E, which promotes the reduction of CeO_2.

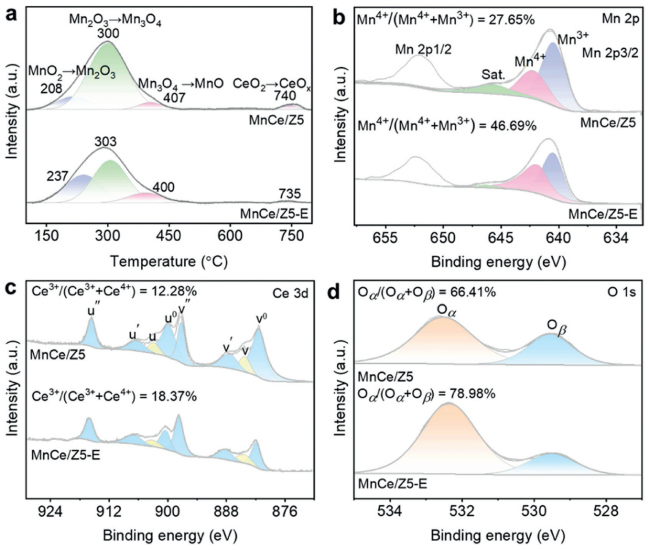

Fig. 3. (a) H_2-TPR profiles of MnCe/Z5-E and MnCe/Z5 catalysts. Mn 2p (b), Ce 3d (c), and O 1s (d) XPS spectra of MnCe/Z5-E and MnCe/Z5 catalysts.

To explore the electronic structure of Mn and Ce over MnCe/Z5-E and MnCe/Z5 catalysts, X-ray photoelectron spectroscopy (XPS) experiments were performed. As seen in Fig. 3b, there are two broad peaks in the range of 635–660 eV, which can be attributed to Mn $2p_{3/2}$ and Mn $2p_{1/2}$. The peak of Mn $2p_{3/2}$ can be assigned to three peaks at 639.6, 642.2, and 645.4 eV, belonging to Mn^{3+}, Mn^{4+}, and satellite peaks respectively [42-44]. By calculating the respective peak area to calculate the relative atomic content of Mn species. It can be found that the ratio of $Mn^{4+}/(Mn^{4+}+Mn^{3+})$ is much higher on MnCe/Z5-E (46.69%) than MnCe/Z5 (27.65%) (Table S4 in Supporting information), indicating that more Mn species with high valence exist on MnCe/Z5-E, which is following the result of H_2-TPR experiments. It has been reported that Mn^{4+} species have a higher oxidative capability than Mn^{3+}, which is beneficial to produce NH_2, NH, and N resulting from the oxidative dehydrogenation of NH_3. Furthermore, NH_2 could interact with gaseous NO to generate N_2 while NH species interact with gaseous NO to generate N_2O [45,46]. The Ce 3d XPS spectra of catalysts are analyzed (Fig. 3c) and can be divided into eight peaks. The peaks denoted as u", u', u^0, v", v', and v^0 are attributed to Ce^{4+}, while the remaining peaks assigned as u and v are belonged to Ce^{3+}, respectively [47]. Notably, the proportion of $Ce^{3+}/(Ce^{4+}+Ce^{3+})$ is also higher on MnCe/Z5-E (18.37%) than on MnCe/Z5 (12.28%) (Table S4 in Supporting information). The higher Ce^{3+} content of MnCe/Z5-E is mainly due to the presence of more Mn^{4+} on the surface according to the chemical equation ($Ce^{4+}+Mn^{3+} \leftrightarrow Ce^{3+}+Mn^{4+}$) and the transfer of electrons from Mn to Ce, which also results in more Mn^{4+} species. This also indicates the strong interaction between Mn and Ce species on MnCe/Z5-E. The higher content of Ce^{3+} in the catalysts can generate more oxygen vacancies that facilitate oxygen migration and promote the reactant molecules' activation. The O 1s XPS spectra of catalysts are further analyzed (Fig. 3d) and can be divided into two peaks, one peak of binding energy of 529.4 eV vests in lattice oxygen (O_β), and the other peak of binding energy of 532 eV belongs to surface adsorption oxygen (O_α) [48]. The proportion of $O_\alpha/(O_\alpha+O_\beta)$ is much higher on MnCe/Z5-E (78.98%) than MnCe/Z5 (66.41%) (Table S4 in Supporting information). O_α is thought to have better oxidation capacity and mobility than lattice oxygen in the redox reaction. Besides, O_2-TPD-MS experiments were employed to explore the mobility of oxygen species of MnCe/Z5-E and MnCe/Z5 (Fig. S14 in Supporting information). Below 200 °C is assigned to the desorption of chemisorbed oxygen over the surface, 200–600 °C belongs to the release of oxygen from the surface lattice, and above 600 °C is due to the release of oxygen from the bulk lattice [49]. MnCe/Z5-E exhibits a distinct desorption peak below 200 °C compared with MnCe/Z5, which indicates that more oxygen species are adsorbed on the surface of MnCe/Z5-E, which is following the XPS results of O 1s. Based on the above results, it can be found that MnCe/Z5-E owns more Mn^{4+} species and stronger oxidative capacity together with more oxygen vacancy and reactive adsorbed oxygen species than MnCe/Z5. Generally, the strong oxidative ability of Mn-based catalysts leads to poor N_2 selectivity because of excessive oxidation of NH_3. However, MnCe/Z5-E shows better N_2 selectivity than MnCe/Z5, indicating the excessive oxidation of NH_3 is inhibited on MnCe/Z5-E.

To explore the natural reason for better N_2 selectivity of MnCe/Z5-E, the acidic properties of catalysts were further investigated because the acidity of catalysts is another critical parameter influencing the activity of catalysts. Fig. 4a shows the NH_3-TPD-MS results of MnCe/Z5-E and MnCe/Z5. The peaks at 205–218 °C belong to weak acid sites, the peaks at 258–264 °C are assigned to moderate-strong acid sites, and the remaining peaks at 356–373 °C representing strong acid sites are discovered above MnCe/Z5-E and

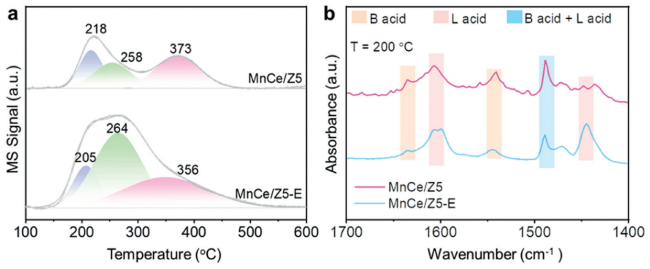

Fig. 4. NH_3-TPD-MS profiles (a) and pyridine-FTIR spectra (b) with pyridine desorption at 200 °C of MnCe/Z5-E and MnCe/Z5 catalysts.

MnCe/Z5 [50]. The amounts of different kinds of acid are quantified, as shown in Table S5 (Supporting information). Notably, MnCe/Z5-E shows much more moderate-strong acid and strong acid sites than MnCe/Z5. The above results show that the surface acidity of MnCe/Z5-E is effectively improved by mixed-alkaline etching, which derives from the etching of Si in the ZSM-5 framework remaining more Al acidic centers (Table S1 in Supporting information). *In situ* DRIFT spectra of NH_3 desorption also indicate that the acidity of the catalyst is enhanced significantly by alkaline treatment, which is consistent with the NH_3-TPD-MS results (Fig. S15 in Supporting information). The acid sites types are further researched on MnCe/Z5-E and MnCe/Z5 by using Pyridine-FTIR (Fig. 4b). The peaks at 1450 and 1600 cm^{-1} represent Lewis acid sites, the peaks at 1540 and 1640 cm^{-1} belong to Brønsted acid sites, and the remaining peak at 1490 cm^{-1} is assigned to both Lewis acid and Brønsted acid sites [51]. It can be found that Lewis acid sites and Brønsted acid sites all exist on MnCe/Z5-E and MnCe/Z5, whereas the MnCe/Z5-E possesses more Lewis acid sites than the unetched MnCe/Z5. As we all know, the Lewis acid sites are closely related to the adsorption of NH_3 species and Brønsted acid sites are responsible for the adsorption of NH_4^+ species in NH_3-SCR. As mentioned before, N_2O could be generated from NH species reacting with gaseous NO *via* the E-R pathway, where NH species derive from the oxidative dehydrogenation of NH_3. Besides, N_2O could be also generated from the decomposition of NH_4NO_3 that derives from the reaction between adsorbed NH_4^+ and NO_3^- species *via* the Langmuir–Hinshelwood (L-H) mechanism [52]. Therefore, the different N_2O formation amount of MnCe/Z5-E and MnCe/Z5 is likely attributed to the more NH_3 species on MnCe/Z5-E and more NH_4^+ species on MnCe/Z5.

$NO + O_2$-TPD-MS experiments were tested to study the adsorption and activation of NO_x. As seen in Fig. S16 (Supporting information), both MnCe/Z5-E and MnCe/Z5 show three fitted peaks, in which the peaks below 220 °C are attributed to the physically adsorbed NO species, and the remaining peaks above 250 °C are ascribed to bridged nitrates and bidentate nitrates species, respectively [9]. It can be found that the desorption peak area of the MnCe/Z5-E is much larger than MnCe/Z5 while the desorption temperature of the MnCe/Z5-E is lower than MnCe/Z5, indicating that MnCe/Z5-E adsorbs more nitrogen oxide species that are also more reactive than MnCe/Z5. *In situ* DRIFTs of NO adsorption also indicate that more nitrogen oxide species adsorb on MnCe/Z5-E than MnCe/Z5.

For the MnCe/Z5-E, the bidentate nitrate (1562 cm^{-1}), bridged nitrate (1631 cm^{-1}), gaseous NO (1691 cm^{-1}), and trans-$N_2O_2^{2-}$ (1724 cm^{-1}) are observed on the surface of MnCe/Z5-E [53-55]. As for the MnCe/Z5, the bridged nitrite (1225 cm^{-1}), bidentate nitrate (1565 cm^{-1}), bridged nitrate (1631 cm^{-1}), and N_2O_4 species (1698 cm^{-1}) are found on MnCe/Z5. It can also be found that the peak strength for nitrate adsorption of MnCe/Z5-E is significantly stronger than MnCe/Z5, which indicates that more nitrogen oxide species adsorb on MnCe/Z5-E than MnCe/Z5 (Fig. S17 in Supporting information). *In situ* DRIFT spectra of NO_x desorption also verify that MnCe/Z5-E has stronger NO_x adsorption ability, which is consistent with the results of $NO + O_2$-TPD-MS (Fig. S18 in Supporting information).

To further explore the NH_3-SCR reaction and N_2O inhibition mechanism of MnCe/Z5-E and MnCe/Z5, *in situ* DRIFT spectra of transient reactions between pre-adsorbed NH_3 and $NO + O_2$ at 150 °C were investigated for MnCe/Z5-E and MnCe/Z5, as seen in Figs. 5a and b. As for MnCe/Z5-E (Fig. 5a), the pre-adsorbed NH_3 results in the appearance of the NH_3 (1195 and 1600 cm^{-1}) and NH_4^+ (1656 cm^{-1}) species [56-58]. After introducing $NO + O_2$, these adsorbed NH_x species were gradually reduced. Meanwhile, the nitrogen oxide species including the M-NO_2 nitrate species (1320 cm^{-1}), the bidentate nitrate (1562 cm^{-1}), bridged nitrate (1627 and 1645 cm^{-1}), and trans-$N_2O_2^{2-}$ (1732 cm^{-1}) [53-55] gradually appear, and the intensity of these bands gradually increases over time. For MnCe/Z5 (Fig. 5b), the pre-adsorbed NH_3 also results in the appearance of NH_3 (1190 and 1600 cm^{-1}) and NH_4^+ species (1660 cm^{-1}) [56-58]. After introducing $NO + O_2$, these adsorbed NH_x species were gradually reduced too, and the nitrogen oxide species including the M-NO_2 nitrate species (1345 cm^{-1}), bidentate nitrate (1565 cm^{-1}), and bridged nitrate (1628 cm^{-1}) [53-55] increase at the same time. The depletion rates of adsorbed NH_x species are compared as shown in Fig. 5c. For MnCe/Z5-E, the NH_4^+ species are almost inactive while the NH_3 species are much more reactive. As for MnCe/Z5, both NH_3 and NH_4^+ species are reactive. Such a result implies that NH_3 species are the predominant reactive intermediate for MnCe/Z5-E while NH_3 and NH_4^+ species are both the reactive intermediate for MnCe/Z5.

In situ DRIFTs of transient reactions between pre-adsorbed $NO + O_2$ and NH_3 at 150 °C of MnCe/Z5-E and MnCe/Z5 catalysts were also recorded, as shown in Figs. 5d and e. As for MnCe/Z5-E (Fig. 5d), the bidentate nitrate (1562 cm^{-1}), bridged nitrate (1631 cm^{-1}), gaseous NO (1691 cm^{-1}), and trans-$N_2O_2^{2-}$ (1724 cm^{-1}) [53-55] appear after the pre-adsorbed $NO + O_2$. After introducing NH_3, the bidentate nitrate and bridged nitrate (1631 cm^{-1}) species gradually disappear while the NH_3 (1176, 1275, and 1600 cm^{-1}) and -NH_2 (1532 and 1719 cm^{-1}) [56-58] species gradually appear. From the aforementioned findings, we can deduce that the reaction may proceed between NH_3 species and adsorbed nitrate species through the L-H mechanism and between -NH_2 species and gaseous NO through the E-R mechanism of MnCe/Z5-E. For MnCe/Z5 (Fig. 5e), the bridged nitrite (1225 cm^{-1}), bidentate nitrate (1565 cm^{-1}), bridged nitrate (1631 cm^{-1}), and N_2O_4 (1698 cm^{-1}) [53-55] species increase after the pre-adsorbed $NO + O_2$. After introducing NH_3, the bidentate nitrate and bridged nitrate species gradually reduce and the NH_3 species (1190, 1270, and 1600 cm^{-1}), NH_4^+ (1735 cm^{-1}), and -NH_2 (1538 cm^{-1}) [56-58] increase at the same time. Based on the aforementioned findings, we can also infer that the reaction may proceed between NH_3/NH_4^+ species and adsorbed nitrate species through the L-H mechanism and between -NH_2 species and gaseous NO *via* the E-R mechanism. It can also be noticed that the consumption rates of bridged nitrate species are significantly much faster than that of bidentate nitrate species on both MnCe/Z5 and MnCe/Z5-E (Fig. 5f), indicating the bridged nitrate species are more reactive for both catalysts in the L-H reaction pathways. Obviously, MnCe/Z5-E and MnCe/Z5 exhibit similar reaction pathways but the difference is that NH_3 species are the predominate reactive intermediate for MnCe/Z5-E while NH_3 and NH_4^+ species are both the reactive intermediate for MnCe/Z5. As seen in Fig. 6, the NH_4^+ species could react with adsorbed nitrate species to form NH_4NO_3 intermediates that directly decompose to N_2O and H_2O at high temperatures, which is likely the natural reason for worse N_2 selectivity of MnCe/Z5 catalyst. As a comparison, MnCe/Z5-E exhibits better N_2 selectivity because the

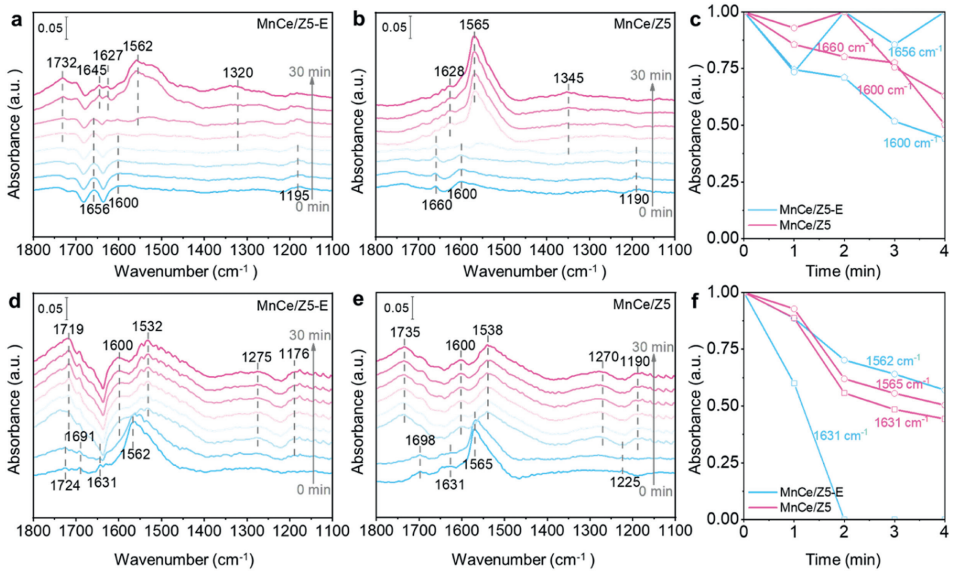

Fig. 5. *In situ* DRIFT spectra of the transient reactions at 150 °C between pre-adsorbed NH_3 and $NO + O_2$ as a function of time over MnCe/Z5-E (a) and MnCe/Z5 (b) catalysts (Experimental conditions: 1000 ppm NH_3, 1000 ppm NO, 5 vol% O_2, N_2 as the balance gas). (c) Plots of normalized intensity of adsorbed NH_x species as a function of time on MnCe/Z5-E and MnCe/Z5 catalysts. *In situ* DRIFT spectra of the transient reactions at 150 °C between pre-adsorbed $NO + O_2$ and NH_3 as a function of time over MnCe/Z5-E (d) and MnCe/Z5 (e) catalysts (Experimental conditions: 1000 ppm NO, 1000 ppm NH_3, 5 vol% O_2, N_2 as the balance gas). (f) Plots of normalized intensity of adsorbed nitrate species as a function of time on MnCe/Z5-E and MnCe/Z5 catalysts.

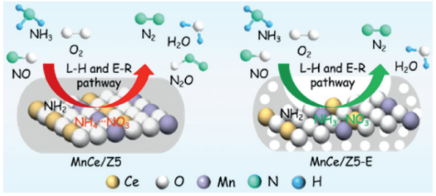

Fig. 6. Schematic diagram of the NH_3-SCR reaction and N_2O inhibition mechanism over MnCe/Z5-E and MnCe/Z5 catalyst.

adsorbed NH_3 species could react with nitrate species to generate N_2 and H_2O while the formed -NH_2 could also react with gaseous NO to generate N_2 and H_2O.

In summary, the etched MnCe/Z5-E catalyst shows above 90% NO_x conversion from 180 °C to 330 °C, which exhibits much better low-temperature activity than the commercial Cu-SSZ-13. Moreover, N_2 selectivity of MnCe/Z5-E is above 80% within the whole temperature window which is much better than the unetched MnCe/Z5. The etched MnCe/Z5-E has a higher surface area and more mesopores, leading to more dispersed state of $MnCeO_x$ species than that on MnCe/Z5. The strong interaction between Mn and Ce species over MnCe/Z5-E promotes the reduction of CeO_2, facilitates the electron transfer from Mn to Ce, and generates more Mn^{4+} and Ce^{3+} species. MnCe/Z5-E owns stronger redox capacity than MnCe/Z5, which contributes to forming the reactive nitrate species and -NH_2 species from oxidative dehydrogenation of NH_3. Moreover, MnCe/Z5-E has more moderate-strong acid and strong acid sites than MnCe/Z5. MnCe/Z5-E exhibits better N_2 selectivity because the adsorbed NH_3 and -NH_2 species are the reactive intermediates that promote the formation of N_2. However, the NH_4^+ species are the main reactive intermediates for MnCe/Z5 that react with adsorbed nitrate species to form NH_4NO_3 and further decompose to N_2O, which is the natural reason for the worse N_2 selectivity. This work demonstrates an effective strategy to improve the low-temperature activity and N_2 selectivity of SCR catalysts, contributing to designing efficient deNO_x catalysts for low-temperature exhaust gas during the cold-start of diesel vehicles.

Declaration of competing interest

All authors declare that there are no conflicts of interest, financial or otherwise in this work; and there are no other relationships or activities that can appear to have influenced the submitted work.

CRediT authorship contribution statement

Shanyuan Bi: Writing – original draft, Data curation. **Jin Zhang:** Writing – original draft, Data curation. **Dengchao Peng:** Data curation. **Danhong Cheng:** Writing – review & editing. **Jianping Zhang:** Writing – review & editing, Conceptualization. **Lupeng Han:** Writing – review & editing, Funding acquisition, Conceptualization. **Dengsong Zhang:** Writing – review & editing, Supervision, Funding acquisition, Data curation, Conceptualization.

Acknowledgments

We acknowledge the National Natural Science Foundation of China (Nos. 22125604, 22106100, 21976117, 22276119) and Shanghai Rising-Star Program (No. 22QA1403700).

Supplementary materials

Supplementary material associated with this article can be found, in the online version, at doi:10.1016/j.cclet.2024.110295.

References

[1] A. Richter, J.P. Burrows, H. Nüß, C. Granier, U. Niemeier, Nature 437 (2005) 129–132.
[2] L. Han, S. Cai, M. Gao, et al., Chem. Rev. 119 (2019) 10916–10976.
[3] W. Chen, R. Zou, X. Wang, ACS Catal. 12 (2022) 14347–14375.
[4] I. Song, H. Lee, S.W. Jeon, et al., Nat. Commun. 12 (2021) 901.
[5] F. Wang, P. Wang, J. Zhang, et al., Chin. Chem. Lett. 35 (2024) 108800.
[6] C. Paolucci, I. Khurana, A.A. Parekh, et al., Science 357 (2017) 898–903.
[7] W. Hu, J. He, X. Liu, et al., Environ. Sci. Technol. 56 (2022) 5170–5178.
[8] L. Yan, F. Wang, P. Wang, et al., Environ. Sci. Technol. 54 (2020) 7697–7705.
[9] X. Liu, P. Wang, Y. Shen, et al., ACS Catal. 12 (2022) 11306–11317.
[10] X. Guo, Z. Ding, N. Kang, et al., Fuel 361 (2024) 130694.
[11] Y. Li, G. Li, Y. Zou, et al., Appl. Catal. B Environ. 344 (2024) 123612.

[12] A. Marberger, A.W. Petrov, P. Steiger, et al., Nat. Catal. 1 (2018) 221–227.
[13] S. Zhang, L. Pang, Z. Chen, et al., Appl. Catal. A: Gen. 607 (2020) 117855.
[14] S. Xie, W. Tan, Y. Li, et al., ACS Catal. 12 (2022) 2441–2453.
[15] B.S. Kim, H. Jeong, J. Bae, et al., Appl. Catal. B: Environ. 270 (2020) 118871.
[16] Z. Chen, Z. Li, Y. Zhang, et al., Chem. Eng. J. 388 (2020) 124322.
[17] L. Pang, C. Fan, L. Shao, et al., Chem. Eng. J. 253 (2014) 394–401.
[18] Q. Zou, M. Liu, M. Fan, et al., J. Rare. Earths 39 (2021) 409–418.
[19] G. Qi, Y. Wang, R.T. Yang, Catal. Lett. 121 (2008) 111–117.
[20] X. Guo, R. Zhang, Z. Di, et al., Appl. Catal. B: Environ. 343 (2024) 123519.
[21] P. Chen, M. Jabłońska, P. Weide, et al., ACS Catal. 6 (2016) 7696–7700.
[22] H. Jouini, I. Mejri, C. Petitto, et al., Micro. Meso. Mater. 260 (2018) 217–226.
[23] B. Liu, K. Zheng, Z. Liao, et al., Ind. Eng. Chem. Res. 59 (2020) 8592–8600.
[24] C. Peng, R. Yan, H. Peng, et al., J. Hazard. Mater. 385 (2020) 121593.
[25] J. Shi, Y. Zhang, Z. Fan, et al., Ind. Eng. Chem. Res. 57 (2018) 13703–13712.
[26] H. Wang, J. Jia, S. Liu, et al., Environ. Sci. Technol. 55 (2021) 5422–5434.
[27] D.A. Peña, B.S. Uphade, P.G. Smirniotis, J. Catal. 221 (2004) 421–431.
[28] J. Ji, Y. Tang, L. Han, et al., Chem. Eng. J. 445 (2022) 136530.
[29] L. Chen, S. Ren, L. Liu, et al., J. Environ. Chem. Eng. 10 (2022) 107167.
[30] G. Zhou, B. Zhong, W. Wang, et al., Catal. Today 175 (2011) 157–163.
[31] L. Yan, S. Chen, P. Wang, et al., Chin. Chem. Lett. 35 (2024) 109132.
[32] J. Xiao, M. Wang, Y. Wang, et al., Ind. Eng. Chem. Res. 61 (2022) 18382–18389.
[33] S. Yuanyuan, Z. Li, X. Zhou, et al., Appl. Catal. B: Environ. 346 (2024) 123747.
[34] J. Han, J. Cho, J.-C. Kim, R. Ryoo, ACS Catal. 8 (2018) 876–879.
[35] Z. Wang, R. Zhang, J. Wang, et al., Fuel 313 (2022) 122669.
[36] F. Bin, C. Song, G. Lv, et al., Appl. Catal. B: Environ. 150-151 (2014) 532–543.
[37] K. Qiao, X. Shi, F. Zhou, et al., Appl. Catal. A: Gen. 547 (2017) 274–282.
[38] J.B. Macstre, E.F. López, J.M. Gallardo-Amores, et al., Inter. J. Inorg. Mater. 3 (2001) 889–899.
[39] Y. Lee, G. He, A.J. Akey, et al., J. Am. Chem. Soc. 133 (2011) 12952–12955.
[40] Y. Yang, X. Liu, Z. Sui, et al., Mol. Catal. 524 (2022) 112284.
[41] L. Jiang, Q. Liu, G. Ran, et al., Chem. Eng. J. 370 (2019) 810–821.
[42] L. Wang, H. He, C. Zhang, et al., Chem. Eng. J. 288 (2016) 406–413.
[43] L. Liu, S. Su, D. Chen, et al., Fuel 307 (2022) 121805.
[44] D. Meng, W. Zhan, Y. Guo, et al., ACS Catal. 5 (2015) 5973–5983.
[45] Y. Gao, Z. Han, G. Zhai, et al., J. Taiwan Inst. Chem. E 133 (2022) 104269.
[46] J. Yang, S. Ren, Y. zhou, et al., Chem. Eng. J. 397 (2020) 125446.
[47] H. Zhang, Z. Li, T. Liu, et al., Environ. Sci. Technol. 56 (2022) 3596–3603.
[48] Q. Wang, Y. Li, A. Serrano-Lotina, et al., J. Am. Chem. Soc. 143 (2021) 196–205.
[49] G. Carja, Y. Kameshima, K. Okada, C.D. Madhusoodana, Appl. Catal. B: Environ. 73 (2007) 60–64.
[50] X. Huang, F. Dong, G. Zhang, et al., Chem. Eng. J. 419 (2021) 129572.
[51] W. Hong, Y. Liu, T. Zhu, et al., Environ. Sci. Technol. 56 (2022) 15695–15704.
[52] L. Chen, S. Ren, Y. Jiang, et al., Fuel 320 (2022) 123969.
[53] Q. Zhang, J. Fan, P. Ning, et al., Appl. Surf. Sci. 435 (2018) 1037–1045.
[54] J. Wang, Z. Yan, L. Liu, et al., Appl. Surf. Sci. 313 (2014) 660–669.
[55] K. Zha, S. Cai, H. Hu, et al., J. Phys. Chem. C 121 (2017) 25243–25254.
[56] I. Song, H. Lee, S.W. Jeon, D.H. Kim, J. Catal. 382 (2020) 269–279.
[57] Y. Zhang, Y. Peng, K. Li, et al., ACS Catal. 9 (2019) 6137–6145.
[58] Z. Liu, S. Zhang, J. Li, L. Ma, Appl. Catal. B: Environ. 144 (2014) 90–95.